Robust Scheduling for Wireless Charger Networks

Xiaoyu Wang*, Haipeng Dai*, He Huang†, Yunhuai Liu‡, Guihai Chen*, Wanchun Dou*
*State Key Laboratory for Novel Software Technology, Nanjing University, Nanjing, Jiangsu 210023, China
†School of Computer Science and Technology, Soochow University, Suzhou, Jiangsu 215006, China
‡Peking University, Beijing 10080, China
Emails: xiaoyuwang18@smail.nju.edu.cn,{haipengdai, gchen, douwc}@nju.edu.cn,
huangh@suda.edu.cn, yunhuai.liu@gmail.com

***Abstract*—In this paper, we deal with the problem of Robust schedUling for wireLess charger nEtworks (RULE), *i.e.*, given a number of rechargeable devices, each of which may drift within a certain range, and a number of directional chargers with fixed positions and adjustable orientations distributed on a 2D plane, determining the orientations of the wireless chargers to maximize the overall expected charging utility while taking the charging power jittering into consideration. To address the problem, we first model the charging power as a random variable, and apply area discretization technique to divide the charging area into several subareas to approximate the charging power as the same random variable in each subarea and bound the approximation error. Then, we discretize the orientations of chargers to deal with the unlimited searching space of orientations with performance bound. Finally, by proving the submodularity of the problem after the above transformations, we propose an algorithm that achieves $(\frac{1}{2}-\epsilon)$-approximation ratio. We conduct both simulation and field experiments, and the results show that our algorithm can perform better than other comparison algorithms by 103.25% on average.**

I. Introduction

Wireless Power Transfer (WPT) technology demonstrates its importance in our daily life due to its convenience such as no wiring, no contact, reliable and continuous power supply, and ease of maintenance, and attracts attentions from not only academic research but also industrial field. Wireless Power Consortium [1], which aims to promote the standardization of WPT, has grown to include 606 companies in 2018, and this number is more than twice of that of last year. In a WPT system, chargers transfer power to rechargeable devices via wireless with reasonable efficiency. Almost all existing works regarding WPT systems focus on performance optimization issues in determined environments, such as deploying specified number of chargers to maximize charging utility/flow rate for pre-deployed sensor networks [2]–[5].

In practice, however, the charging environments are always highly dynamic with uncertainties. A WPT system should be sufficiently robust to deal with such dynamics. Such dynamics are mainly due to the following reasons. First, instead of the traditional static WSNs [6], [7], the wireless devices may drift since they are not absolutely fixed; example cases include but not limited to: (1) devices can drift in their task areas to expand the scope of monitoring [8]; (2) sensors in pipe networks may drift when flow passes [9]; (3) non-fixed sensors [10] like underwater sensors [11] and sensors on unmanned aerial vehicles [12] may drift without control; (4) the sensors on bridges to monitor structural health are required to detect acceleration, ambient vibration and so on [13] so they may slightly drift with vibration. These drift cases may cause these devices out of charging area and decrease the network lifetime if cases are in wireless rechargeable sensor networks. Second, the charging power jitters [14], which means the charging power is not a certain value for a certain pair of charger and device. Unfortunately, recent works about wireless charger scheduling always do not consider these uncertainties.

In this paper, we deal with the problem of Robust schedUling for wireLess charger nEtworks (RULE), *i.e.*, given a number of rechargeable devices, each of which may drift within a certain range, and a number of directional chargers with fixed positions and adjustable orientations distributed on a 2D plane, determining the orientations of the wireless chargers to maximize the overall charging utility while taking the charging power jittering into consideration.

Related works about our problem mainly involve robust wireless charging problem and wireless charger placement/scheduling problem. The former work only considers the jittering of electromagnetic radiation (EMR) rather than charging power while the latter works just apply deterministic models, which are not fit to our problem.

There are four main challenges in our problem. First, the charging power jitters rather than be a static value for a point on the plane, which raises the challenge to evaluate the charging power and even the charging utility. Second, the charging power is nonlinear with distance and it is additive from different chargers for one device, thus, the problem cannot be regarded as a simple geometric coverage problem. Third, it is a continuous problem that we should take the whole area into consideration where these devices can drift rather than only consider limited number of positions of devices as in static topologies. Fourth, infinite orientations for chargers to choose leads to the unlimited solution space.

To address the problem, for the first challenge, we model the charging power as a random variable and these random variables of the charging power from different chargers are independent. We take the expectation of charging utility, a monotone increasing concave function of charging power, as the measurement. For the second one, we apply area discretization to divide the charging area of chargers into several subareas to approximate the charging power as the same random variable in each subarea. For the third one,

TABLE I
NOTATIONS

Symbol	Meaning
s_i	The ith wireless charger, or its position
o_j	The jth wireless rechargeable device
O_j	The DDA of wireless rechargeable device o_j
O_j^k	The kth subarea of O_j
p_j	The DDA center of wireless rechargeable device o_j
r_o	The radius of DDA
N	Number of chargers
M	Number of devices
α	Charging angle of chargers
φ_i	Orientation of charger o_i
$P_w(.)$	Charging power function (a random variable)
$g_X(.)/\tilde{g}_X(.)$	Probability density function/approximated probability density function of selected strategies in set X
P_{th}	Threshold for charging utility function
a_1, b_1, a_2, b_2	Constants in the charging model
D	Farthest distance chargers can reach
$\mathcal{U}(.)$	Utility function
$A(.)$	Area function

the drifting areas of devices can also be divided into several subareas based on area discretization due to geometric symmetry, where expected charging power and charging utility are constant. Thus, we only need to calculate the expected charging utility in each subarea. For the fourth one, we discretize the orientations of chargers into limited ones with performance bound. By proving the submodularity, we use greedy algorithm to achieve $(\frac{1}{2}-\epsilon)$-approximation ratio.

We conduct both simulation and field experiments to evaluate our algorithm. Results show that our algorithm can outperform other comparison algorithms by 103.25% on average.

II. Related Work

As far as we know, almost all the existing works regarding static robust wireless charging schemes do not consider power jittering or device position uncertainty in the objective function. Only work [14] applies probabilistic model to portray the jittering property of electromagnetic radiation (EMR), which aims to schedule the power of chargers to control EMR value. However, the charging power is evaluated as a deterministic value as its expectation so that the technology cannot be applied to address our problem.

Others include wireless charger placement/scheduling problem. Generally, the existing related works can be divided into two folds: ones adopting omnidirectional charging model and those adopting directional charging model. The former models the charging area of chargers and power receiving area of devices as disks [15]–[21]. The latter models the charging area/receiving area as sectors [2], [3], [22]–[25]. All these works apply deterministic models which are not fit to ours.

III. Problem Formulation

A. Network Model and Charging Model

Suppose there are M omnidirectional rechargeable devices $O=\{o_1,...,o_M\}$ and N directional chargers $S=\{s_1,...,s_N\}$ placed on a 2D plane Ω. Without confusion, we also use s_i $(i=1,...,N)$ to denote the position of the ith charger in Ω. The chargers are fixed at their positions s_i $(i=1,...,N)$ but their orientations are freely adjustable. We assume that the rechargeable devices can drift within a certain range, denoted as the Drifting Disk Area (DDA), and p_j is the center of the DDA of o_j $(j=1,...,M)$. We further assume that o_j can be anywhere in the disk with a uniform distribution because of the practical concerns.

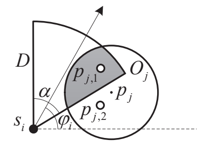

Fig. 1. Charging model

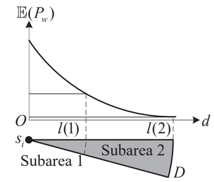

Fig. 2. Power approximation

We build our charging model based on empirical studies [2], [3]. The charging area of a directional charger can be modeled as a sector with radius D. As shown in Figure 1, charger s_i has its orientation angle φ_i and a charging angle α. We consider the typical case that the charging angle $\alpha\in(0,\frac{\pi}{2}]$ due to the strong directional property of directional chargers. For example, the TX91501 power transmitter produced by Powercast [26] provides a charging angle of about 60° [2]. If the position $p=(x,y)$ of the device o_j is in the charger's charging area, it can always receive non-zero charging power, and none for otherwise. In Figure 1, o_j can always harvest non-zero charging power at position $p_{j,1}$ but cannot at position $p_{j,2}$. In addition, the charging power from a charger jitters due to multipath effect, so that we model it as a random variable [14]. By combining the widely used directional charging model and the probabilistic power model in [14], we can formalize our charging model as follows.

$$P_w(s_i,\varphi_i,p)\begin{cases}\sim\mathcal{N}\left(\dfrac{a_1}{(d(s_i,p)+b_1)^2},\left[\dfrac{a_2}{(d(s_i,p)+b_2)^2}\right]^2\right), & \\ \quad d(s_i,p)\le D & \\ \quad \text{and } \overrightarrow{s_ip}\cdot(\cos\varphi_i,\sin\varphi_i)-d(s_i,p)\cos\dfrac{\alpha}{2}\ge 0, & \\ 0, \quad \text{otherwise}, & \end{cases} \tag{1}$$

where a_1,b_1,a_2,b_2 are four parameters decided by the hardware and the environment and $d(s_i,p)$ denotes the distance between charger s_i and the device position p. The model shows that if the device is in the charging sector area of the charger, the receiving power obeys a normal distribution of which the parameters are related to the distance between the charger and the device. Moreover, we assume that the charging power from multiple chargers is additive, that is,

$$P_w(p)=\sum_{i=1}^{N}P_w(s_i,\varphi_i,p). \tag{2}$$

B. Charging Utility Model

We define a charging utility model considering that the power harvesting process may gradually slow down for each rechargeable device [3], [27], [28]. To generalize, the charging utility function $\mathcal{U}(x)$, where x denotes charging power, is a monotone increasing concave function when $x\ge 0$; it equals 0, otherwise. To normalize, we suppose that $\mathcal{U}(x)$ converges to 1 or finally reaches 1 without increasing any more. Since charging power is a random variable, charging utility of charging power is also a random variable. Here we use a linear bounded function to define $\mathcal{U}(.)$.

$$\mathcal{U}(x)=\begin{cases}0, & x\le 0,\\ x/P_{th}, & 0<x\le P_{th},\\ 1, & x>P_{th},\end{cases} \tag{3}$$

where P_{th} is the power threshold which denotes rechargeable devices cannot harvest power any more when they have already received P_{th} power.

C. Problem Formulation

First, according to Equation (2), the expected charging utility for a rechargeable device o_j at point $p = (x, y) \in O_j$ is $\mathbb{E}[\mathcal{U}(\sum_{i=1}^{N} P_w(s_i, \varphi_i, (x, y)))]$ since there are N chargers in total. Then, the overall expected charging utility for device o_j in its DDA O_j is the normalized sum of the expected charging utility of all the points in O_j. Since there are infinite number of points in an area, it becomes a normalized double integral in area O_j, *i.e.*, $\frac{1}{\pi r_o^2}\iint_{(x,y)\in O_j}\mathbb{E}[\mathcal{U}(\sum_{i=1}^{N} P_w(s_i, \varphi_i, (x, y)))]dxdy$. Finally, there are M devices in total, so we add their overall expected charging utility in their own moving circles together and get the average value. Thus, the problem is formalized as:

$$\begin{aligned}(\textbf{P1}) \max_{\varphi_i}\ & \frac{1}{M\pi r_o^2}\sum_{j=1}^{M}\iint_{(x,y)\in O_j}\mathbb{E}[\mathcal{U}(\sum_{i=1}^{N} P_w(s_i,\varphi_i,(x,y)))]dxdy,\\ \text{s.t. } & O_j\subseteq\Omega,\ \varphi_i\in[0,2\pi),\ i=1,...,N,\ j=1,...,M.\end{aligned} \tag{4}$$

The hardness of the problem is described in the theorem below.

Theorem III.1. *The problem* ***P1*** *is NP-hard.*

We omit some proofs in this paper due to the space limit.

IV. Solution

In this section, we introduce the detailed solution of the problem **P1** which achieves approximation ratio $\frac{1}{2}-\epsilon$. We first apply area discretization to approximate the charging power in the same subarea with performance guarantee to address the nonlinearity of the problem. Then, to confine the unlimited searching space, we also discretize the orientations and bound the covering area gap. Finally, we reformulate the problem as maximizing a monotone submodular function subject to a partition matroid, propose our RULE algorithm, and give the overall performance guarantee.

A. Area Discretization

1) Piecewise Constant Function Approximation: To deal with the continuous and nonlinear charging power expectation, we first approximate the charging power of a charger by a piecewise constant function. Let $P_w(d)$ denote the charging power from a charger to a device with distance d. The piecewise constant function is defined as follows:

$$\widetilde{P_w}(d)=\begin{cases}P_w(l(1)), d=0,\\ P_w(l(k)), l(k-1)<d\le l(k),\ (k=1,...,K),\\ 0, d>D,\end{cases} \tag{5}$$

where $l(K) = D$. As shown in Figure 2, the charging area of charger s_i is divided into two subareas and the charging power is approximated as $P_w(l(k))$ at any point in subarea k ($k = 1, 2$), so that the expected charging power in each subarea is a constant as the horizontal line shows. We use $\widetilde{P_w}(d) = 0$ to denote the fact that the random variable $\widetilde{P_w}(d)$ can only equal to 0, *i.e.*, $\mathrm{P}[\widetilde{P_w}(d) = 0] = 1$. It is obvious that $\widetilde{P_w}(d) = 0$ if and only if $P_w(d) = 0$. In the following lemmas corresponding to approximation error, we only discuss the case that the charger provides non-zero charging power.

2) Charging Utility Approximation for a DDA: The DDA O_j is divided into several subareas by the piecewise constant function in which the approximated expectation and variance of charging power are constant. We denote the kth subarea in O_j as O_j^k.

Lemma IV.1. *Let $\widetilde{P_w}(s_i, \varphi_i, O_j^k)$ denote the approximated charging power received at any point $p = (x, y) \in O_j^k$ from charger s_i with orientation φ_i. By setting $l(0) = 0$,*

$$l(k)=\min\{\sqrt{1+\epsilon_1}\,(l(k-1)+b_1),\sqrt{1+\epsilon_1}\,(l(k-1)+b_2)\},$$

where $k = 1, ..., K-1$ and $l(K) = D$ such that

$$l(K-1)<D\le\min\{\sqrt{1+\epsilon_1}\,(l(K-1)+b_1),\sqrt{1+\epsilon_1}\,(l(K-1)+b_2)\},$$

the approximation error of the expectation of charging utility from all the chargers can be bounded as:

$$1\le\frac{\mathbb{E}[\mathcal{U}(\sum_{i=1}^{N}P_w(s_i,\varphi_i,p))]}{\mathbb{E}[\mathcal{U}(\sum_{i=1}^{N}\widetilde{P_w}(s_i,\varphi_i,O_j^k))]}\le 1+\epsilon_1. \tag{6}$$

3) Problem Reformulation: After charging utility approximation, the problem **P1** is approximated as:

$$\begin{aligned}(\textbf{P2}) \max_{\varphi_i}\ & \frac{1}{M\pi r_o^2}\sum_{j=1}^{M}\sum_{O_j^k\subseteq O_j}\mathbb{E}[\mathcal{U}(\sum_{i=1}^{N}\widetilde{P_w}(s_i,\varphi_i,O_j^k))]A(O_j^k),\\ \text{s.t. } & O_j\subseteq\Omega,\ \varphi_i\in[0,2\pi), i=1,...,N,\end{aligned} \tag{7}$$

where $A(O_j^k)$ denotes the area of O_j^k and $\sum_{O_j^k\subseteq O_j}A(O_j^k) = \pi r_o^2$. $\widetilde{P_w}(s_i, \varphi_i, O_j^k)$ denotes the approximated charging power at any point in subarea O_j^k provided by charger s_i with orientation φ_i.

B. Orientation Discretization

Since the orientation of a charger is a continuous value and the relationship between all the covering subareas and the orientation is difficult to describe, we discretize the orientation into limited number of directions with $\Delta\varphi$ interval and bound the approximation error. We assume $\Delta\varphi$ can be divided by 2π with no remainder for simplicity.

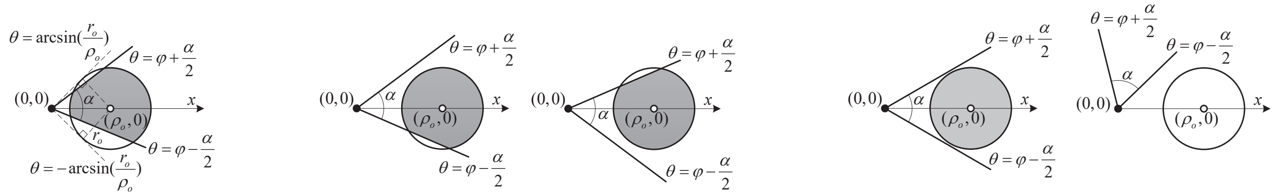

(a) Two line bounds cross the circle (b) One line bound cross the circle (c) None line bound cross the circle

Fig. 3. Charger outside the DDA

Lemma IV.2. *The gap between the original area and the area after orientation discretization covered by one charger in a DDA is bounded as* $2r_o(D+r_o)\Delta\varphi$ *when* $\alpha \in (0, \frac{\pi}{2}]$.

Proof: We prove this lemma under polar coordinate system. First, we give notations and equations of lines and the DDA circle bound. Then, we discuss the three conditions: the charger outside/on/inside the DDA circle bound, respectively. At last, we derive the result.

Since we only consider a pair of charger and device, we do not care the indices of the charger and the device, and write $A(s_i, \varphi_i, O_j)$ as $A(\varphi)$ for simplicity. Suppose the charger is at the pole $(0,0)$ and the device position center is $(\rho_o, 0)$. It should be noticed that any other cases that the device center position is not on the polar axis can be transformed into this situation by rotating the polar axis. The two beams of the charging area are $\theta = \varphi - \frac{\alpha}{2}$ and $\theta = \varphi + \frac{\alpha}{2}$. The DDA circle bound can be described as follows due to cosine theorem.

$$\rho_o^2 + \rho^2 - 2\rho\rho_o\cos\theta = r_o^2. \tag{8}$$

We need to get the function $\rho(\theta)$ to further calculate the covering area. Since the circle is a quadratic equation about ρ, the equation may have two, one, or none root(s), which corresponds to different calculating cases.

We need to explore the maximum change rate of charging area while rotating the charger, that is, the maximum value of $|A'(\varphi)|$. It is obvious that the absolute value of the minimum and maximum $A'(\varphi)$ are the same due to the symmetry of the circle. In most cases, we can calculate the maximum value of $|A'(\varphi)|$ with the φ which satisfies $A''(\varphi) = 0$.

We only consider the two line bounds of the charging area and neglect the farthest arc bound while rotating, since the farthest arc bound of charging area will contribute nothing to the area changing rate so that the area changing rate is smaller.

Charger outside the DDA: In this case, three situations may occur:

1) Both $\theta = \varphi - \frac{\alpha}{2}$ and $\theta = \varphi + \frac{\alpha}{2}$ cross the circle;
2) Only one beam $\theta = \varphi - \frac{\alpha}{2}$ or $\theta = \varphi + \frac{\alpha}{2}$ cross the circle;
3) None of the two beams cross the circle.

These situations can be seen in Figure 3(a)-(c), respectively. In situation 3), the covering area is either the area of the whole circle or 0, and both the changing rates are 0. We only consider the first and the second situations.

Define the two functions of the circle as

$$\rho_1(\theta) = \rho_o\cos\theta + \sqrt{r_o^2 - \rho_o^2\sin^2\theta}, \tag{9}$$

$$\rho_2(\theta) = \rho_o\cos\theta - \sqrt{r_o^2 - \rho_o^2\sin^2\theta}, \tag{10}$$

which are derived from Equation (8). In situation 1), the covering area can be calculated as:

$$\begin{aligned} A(\varphi) &= \int_{\varphi-\frac{\alpha}{2}}^{\varphi+\frac{\alpha}{2}} \frac{1}{2}[\rho_1^2(\theta) - \rho_2^2(\theta)]\, d\theta \\ &= 2\rho_o \int_{\varphi-\frac{\alpha}{2}}^{\varphi+\frac{\alpha}{2}} \cos\theta \cdot \sqrt{r_o^2 - \rho_o^2\sin^2\theta}\, d\theta, \end{aligned} \tag{11}$$

where $-\arcsin\left(\frac{r_o}{\rho_o}\right) < \varphi - \frac{\alpha}{2} < \varphi + \frac{\alpha}{2} < \arcsin\left(\frac{r_o}{\rho_o}\right)$. Let $A''(\varphi) = 0$ and we get the only case $\sin(\varphi - \frac{\alpha}{2}) = \sin(\varphi + \frac{\alpha}{2})$, but the value of φ exceeds its range. Thus, $A'(\varphi)$ must be monotone in its domain. Due to the symmetry, the values of $|A'(\varphi)|$ at the end points of the domain, *i.e.*, $\varphi = -\arcsin(\frac{r_o}{\rho_o}) + \frac{\alpha}{2}$ and $\varphi = \arcsin(\frac{r_o}{\rho_o}) - \frac{\alpha}{2}$, are the same and this value is the upper bound in this situation. That is,

$$\begin{aligned} |A'(\varphi)| &< 2\rho_o|\cos(\alpha - \arcsin(\frac{r_o}{\rho_o}))|\sqrt{r_o^2 - \rho_o^2\sin^2(\alpha - \arcsin(\frac{r_o}{\rho_o}))} \\ &\leq 2\rho_o r_o, \end{aligned} \tag{12}$$

since $|\cos(\alpha - \arcsin(\frac{r_o}{\rho_o}))| \leq 1$ and $\sin^2(\alpha - \arcsin(\frac{r_o}{\rho_o})) \geq 0$.

In situation 2), it is similar to get the upper bound $2\rho_o r_o$.

To conclude, when the charger is outside the DDA, the area changing rate $|A'(\varphi)| \leq 2\rho_o r_o$.

Charger on the DDA circle bound: In this case, the function of DDA circle bound reduces to:

$$\rho(\theta) = 2r_o\cos\theta, \quad \theta \in [-\frac{\pi}{2}, \frac{\pi}{2}], \tag{13}$$

and it is easy to get the bound $|A'(\varphi)| \leq 2\rho_o r_o$. We omit the proof of this case here.

Charger inside the DDA: The covering case can be seen in Figure 5. In this case, we see that there must be one root for ρ in Equation (8) since $r_o > \rho_o$ and we can write $\rho(\theta)$ as:

$$\rho(\theta) = \rho_o\cos\theta + \sqrt{\rho_o^2\cos^2\theta + (r_o^2 - \rho_o^2)}. \tag{14}$$

The covering area $A(\varphi)$ can be calculated as:

$$\begin{aligned} A(\varphi) &= \int_{\varphi-\frac{\alpha}{2}}^{\varphi+\frac{\alpha}{2}} \frac{1}{2}\rho^2(\theta)d\theta \\ &= \frac{1}{2}\int_{\varphi-\frac{\alpha}{2}}^{\varphi+\frac{\alpha}{2}} \left(\rho_o\cos\theta + \sqrt{\rho_o^2\cos^2\theta + (r_o^2 - \rho_o^2)}\right)^2 d\theta. \end{aligned} \tag{15}$$

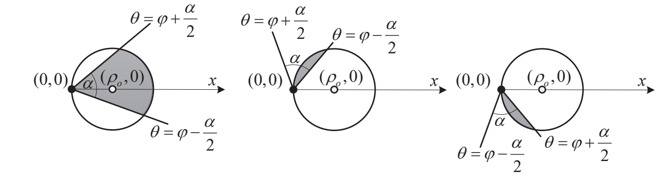

(a) Two line bounds cross the circle (b) One line bound cross the circle (c) None line bound cross the circle

Fig. 4. Charger on the DDA circle bound

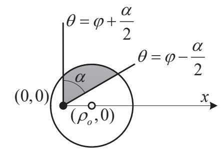

Fig. 5. Charger inside the DDA

Algorithm 1: Robust Scheduling

Input: Candidate orientation set of the ith charger X_i ($i=1,...,N$), charger set $S=\{s_1,...,s_N\}$, device set $O=\{o_1,...,o_M\}$, density function of charging power provided by one charger, utility function $\mathcal{U}(x)$, objective function $f(X)$.

Output: Selected orientation set Γ.

```
Γ = ∅.
X = ⋃_{i=1}^{N} X_i.
while |Γ| < N do
    e* = arg max_{e∈X\Γ} f(X ∪ {e}) − f(X).
    Γ = Γ ∪ {e*}.
    X = X\X_i where e* ∈ X_i.
```

Define

$$A_f(x)=\rho_o x\left(\rho_o x+\sqrt{\rho_o^2x^2+(r_o^2-\rho_o^2)}\right), \quad x\in[-1,1], 0<\rho_o<r_o. \tag{16}$$

Then,

$$\begin{aligned}A'(\varphi)&=A_f(\cos(\varphi+\frac{\alpha}{2}))-A_f(\cos(\varphi-\frac{\alpha}{2}))\\&\leq A_f(1)-A_f(-1)=2\rho_o r_o,\end{aligned} \tag{17}$$

since $A'_f(x)=0$ requires $(\rho_o^2-r_o^2)^2=0$ which cannot be satisfied, and $A'_f(1)>0$, $A'_f(x)>0$ when $x\in[-1,1]$. Thus, $A_f(x)$ ($x\in[-1,1]$) is a monotone increasing function, so we have the upper bound $2\rho_o r_o$.

Therefore, in all the three cases, the area changing rate is no larger than $2\rho_o r_o$. Considering that a charger covering a DDA with non-zero area requires $\rho_o<D+r_o$, the area changing rate is less than $2r_o(D+r_o)$. Thus, the maximum changing area is less than $2r_o(D+r_o)\Delta\varphi$ by rotating $\Delta\varphi$. ■

After orientation discretization, the problem **P2** in Equation (7) is reformulated as:

$$\begin{aligned}(\textbf{P3})\max_{\tilde{\varphi}_i}\ &\frac{1}{M\pi r_o^2}\sum_{j=1}^{M}\sum_{O_j^k\subseteq O_j}\mathbb{E}[\mathcal{U}(\sum_{i=1}^{N}\widetilde{P_w}(s_i,\tilde{\varphi}_i,O_j^k))]A(O_j^k),\\ \text{s.t. }&O_j\subseteq\Omega,\ \tilde{\varphi}_i=n_i\Delta\varphi,\\ &n_i\in\{0,...,\frac{2\pi}{\Delta\varphi}-1\},\ i=1,...,N,\ j=1,...,M.\end{aligned} \tag{18}$$

C. Algorithm and Theoretical Analysis

In this subsection, we will give a $(\frac{1}{2}-\epsilon)$-approximation algorithm and its further analysis. The details of the algorithm is shown in Algorithm 1, which is essentially a greedy algorithm. In the following, we will prove the validity of this algorithm by giving the approximation ratio.

Definition IV.1. *[29] Let S be a finite ground set. A real-valued set function $f:2^S\rightarrow\mathbb{R}$ is normalized, monotonic and submodular if and only if it satisfies the following conditions, respectively: (1) $f(\emptyset)=0$; (2) $f(S_1\cup\{e\})-f(S_1)\geq 0$ for any $S_1\subseteq S$ and $e\in S\backslash S_1$; (3) $f(S_1\cup\{e\})-f(S_1)\geq f(S_2\cup\{e\})-f(S_2)$ for any $S_1\subseteq S_2\subseteq S$ and $e\in S\backslash S_2$.*

Definition IV.2. *[29] **Partition matroid:** Given $S=\bigcup_{i=1}^{k}S'_i$ is the disjoint union of k sets, $l_1,l_2,\ldots,l_k$ are positive integers, a* partition matroid *$\mathcal{M}=(S,\mathcal{I})$ is a matroid where $\mathcal{I}=\{X\subset S:|X\cap S'_i|\leq l_i$ for $i\in[k]\}$.*

The direction set Γ generated by orientation discretization can be defined as the disjoint union of the N direction sets of different chargers, *i.e.*, $\Gamma=\bigcup_{q=1}^{N}\Gamma_q$. Thus, define the partition matroid $\mathcal{M}=(\Gamma,\mathcal{I})$ with $\mathcal{I}=\{X\subset\Gamma:|X\cap\Gamma_q|\leq 1$ for $q\in[N]\}$. Based on the definitions above, problem **P3** can be rewritten as:

(**P4**)

$$\begin{aligned}\max\ f(X)=&\frac{1}{M\pi r_o^2}\sum_{j=1}^{M}\sum_{O_j^k\subseteq O_j}\mathbb{E}[\mathcal{U}(\sum_{\tilde{\varphi}_i\in X}\widetilde{P_w}(s_i,\tilde{\varphi}_i,O_j^k))]A(O_j^k),\\ \text{s.t. }&O_j\subseteq\Omega, X\in L, L=\{X\subseteq\Gamma:|X\cap\Gamma_q|\leq 1\},\ j=1,...,M.\end{aligned} \tag{19}$$

Lemma IV.3. *The objective function $f(X)$ in problem **P4** is a monotone submodular function, and the constraint is a partition matroid constraint.*

Proof: To verify the submodularity of function $f(X)$, we only need to check whether $f(X)$ satisfies the three conditions in Definition IV.1. Define

$$f_1(X,j,k)=\mathbb{E}[\mathcal{U}(\sum_{\tilde{\varphi}_i\in X}\widetilde{P_w}(s_i,\tilde{\varphi}_i,O_j^k))]. \tag{20}$$

Thus, we have

$$f(X)=\frac{1}{M\pi r_o^2}\sum_{j=1}^{M}\sum_{O_j^k\subseteq O_j}f_1(X,j,k)A(O_j^k). \tag{21}$$

Note that the area discretization is different for different charger set X, *i.e.*, O_j^ks are different. To unify the subareas, we discretize the subareas more finely to ensure the different charger sets in the same condition give common subareas.

Further, we define the probability density function for random variable $\sum_{\tilde{\varphi}_i\in X}\widetilde{P_w}(s_i,\tilde{\varphi}_i,O_j^k)$ as $\tilde{g}_X(x)$. Since charging power provided by different chargers is independent, the random variables $\sum_{\tilde{\varphi}_i \in S_1} \widetilde{P_w}(s_i, \tilde{\varphi}_i, O_j^k)$ and $\sum_{\tilde{\varphi}_i \in S_2} \widetilde{P_w}(s_i, \tilde{\varphi}_i, O_j^k)$ are independent if $S_1 \cap S_2 = \emptyset$. That is, the joint probability density function $\tilde{g}_{S_1 \cup S_2}(x, y)$ of the random variable $\sum_{\tilde{\varphi}_i \in S_1 \cup S_2} \widetilde{P_w}(s_i, \tilde{\varphi}_i, O_j^k) = \sum_{\tilde{\varphi}_i \in S_1} \widetilde{P_w}(s_i, \tilde{\varphi}_i, O_j^k) + \sum_{\tilde{\varphi}_i \in S_2} \widetilde{P_w}(s_i, \tilde{\varphi}_i, O_j^k)$ is equal to $\tilde{g}_{S_1}(x)\tilde{g}_{S_2}(y)$.

It is obvious that $f(X)$ satisfies the first and the second conditions with $f(\emptyset) = 0$ and monotonically increasing property. For the third condition, we give a lemma first.

Lemma IV.4. *The monotonically increasing concave function $\mathcal{U}(x)$ has the property that*

$$F_{\mathcal{U}}(x, y, z) = (\mathcal{U}(x+z) - \mathcal{U}(x)) - (\mathcal{U}(x+y+z) - \mathcal{U}(x+y)) \geq 0, \tag{22}$$

where $x, y, z \geq 0$.

By referring to the result in Lemma IV.4, we define

$$\begin{aligned}
&\Delta f_1(S_1, S_2, \{e\}, j, k) \\
&= (f_1(S_1 \cup \{e\}, j, k) - f_1(S_1, j, k)) \\
&\quad - (f_1(S_2 \cup \{e\}, j, k) - f_1(S_2, j, k)) \\
&= \left(\mathbb{E}[\mathcal{U}(\sum_{\tilde{\varphi}_i \in S_1 \cup \{e\}} \widetilde{P_w}(s_i, \tilde{\varphi}_i, O_j^k))] - \mathbb{E}[\mathcal{U}(\sum_{\tilde{\varphi}_i \in S_1} \widetilde{P_w}(s_i, \tilde{\varphi}_i, O_j^k))] \right) \\
&\quad - \Bigg(\mathbb{E}[\mathcal{U}(\sum_{\tilde{\varphi}_i \in S_1 \cup (S_2 \setminus S_1) \cup \{e\}} \widetilde{P_w}(s_i, \tilde{\varphi}_i, O_j^k))] \\
&\qquad - \mathbb{E}[\mathcal{U}(\sum_{\tilde{\varphi}_i \in S_1 \cup (S_2 \setminus S_1)} \widetilde{P_w}(s_i, \tilde{\varphi}_i, O_j^k))] \Bigg) \\
&= \left(\int_{-\infty}^{+\infty}\int_{-\infty}^{+\infty} \mathcal{U}(x+y)\tilde{g}_{S_1}(x)\tilde{g}_{\{e\}}(y)dxdy - \int_{-\infty}^{+\infty} \mathcal{U}(x)\tilde{g}_{S_1}(x)dx \right) \\
&\quad - \left(\int_{-\infty}^{+\infty}\int_{-\infty}^{+\infty}\int_{-\infty}^{+\infty} \mathcal{U}(x+y+z)\tilde{g}_{S_1}(x)\tilde{g}_{S_2 \setminus S_1}(y)\tilde{g}_{\{e\}}(z)dxdydz \right. \\
&\qquad \left. - \int_{-\infty}^{+\infty}\int_{-\infty}^{+\infty} \mathcal{U}(x+y)\tilde{g}_{S_1}(x)\tilde{g}_{S_2 \setminus S_1}(y)dxdy \right) \\
&= \int_0^{+\infty}\int_0^{+\infty}\int_0^{+\infty} F_{\mathcal{U}}(x, y, z)\tilde{g}_{S_1}(x)\tilde{g}_{S_2 \setminus S_1}(y)\tilde{g}_{\{e\}}(z)dxdydz \geq 0.
\end{aligned} \tag{23}$$

Thus,

$$\begin{aligned}
&(f(S_1 \cup \{e\}) - f(S_1)) - (f(S_2 \cup \{e\}) - f(S_2)) \\
&= \frac{1}{M\pi r_o^2} \sum_{j=1}^{M} \sum_{O_j^k \subseteq O_j} \Delta f_1(S_1, S_2, \{e\}, j, k) A(O_j^k) \geq 0.
\end{aligned} \tag{24}$$

That is,

$$f(S_1 \cup \{e\}) - f(S_1) \geq f(S_2 \cup \{e\}) - f(S_2),\ S_1 \subseteq S_2 \subseteq S,\ e \in S \setminus S_2. \tag{25}$$

To sum up, $f(X)$ in Equation (19) is a monotone submodular function and clearly the constraint is a partition matroid constraint. ■

Theorem IV.1. *Setting $\Delta\varphi = \frac{A_w}{2MNr_o(D+r_o)}\epsilon$ and $\epsilon_1 = \frac{\epsilon}{1-\epsilon}$, where*

$$A_w = \begin{cases}
\frac{1}{2}\alpha D^2, \quad D \leq r_o, \\
\frac{1}{2}\alpha D^2 - d_1 D \sin\frac{\alpha}{2} + \arccos(\frac{r_o^2 + D^2 - d_1^2}{2Dr_o}) r_o^2, \\
\qquad D > r_o \text{ and } \sin\frac{\alpha}{2} < \frac{r_o}{D}\sqrt{1 - \frac{r_o^2}{2D^2}}, \\
A_c - 2\left(\arccos(\frac{D\sin\frac{\alpha}{2}}{r_o}) r_o^2 - D\sin\frac{\alpha}{2}\sqrt{r_o^2 - D^2\sin^2\frac{\alpha}{2}} \right), \\
\qquad D > r_o \text{ and } \frac{r_o}{D}\sqrt{1 - \frac{r_o^2}{2D^2}} \leq \sin\frac{\alpha}{2} < \frac{r_o}{D}, \\
A_c, \quad \text{otherwise},
\end{cases} \tag{26}$$

$d_1 = D\cos\frac{\alpha}{2} - \sqrt{r_o^2 - D^2\sin^2\frac{\alpha}{2}}$ and $A_c = D^2\arccos(1 - \frac{r_o^2}{2D^2}) + r_o^2\arccos(\frac{r_o}{2D}) - r_o D\sin(\arccos(1 - \frac{r_o^2}{2D^2}))$, the algorithm achieves an approximation ratio of $\frac{1}{2} - \epsilon$, and the time complexity is $O(M^2N^4\epsilon^{-3})$.

Proof: Let Γ_1^*, Γ_2^*, and Γ_3^* denote the optimal solutions to the problem **P1**, **P2** and **P3** (or **P4**), respectively, and Γ_3 denote the obtained solution to problem **P4**. First, according to Lemma IV.1, the fact that the greedy algorithm of maximizing a monotone submodular function subject to a partition matroid constraint achieves a $\frac{1}{2}$-approximation ratio [29], and Lemma IV.2, we have:

$$\begin{aligned}
&\frac{1}{M\pi r_o^2} \sum_{j=1}^{M} \sum_{O_j^k \subseteq O_j} \mathbb{E}[\mathcal{U}(\sum_{\varphi_i \in \Gamma_2^*} \widetilde{P_w}(s_i, \varphi_i, O_j^k))] A(O_j^k) \\
&\geq \frac{1}{1+\epsilon_1} \cdot \frac{1}{M\pi r_o^2} \sum_{j=1}^{M} \iint_{(x,y) \in O_j} \mathbb{E}[\mathcal{U}(\sum_{\varphi_i \in \Gamma_1^*} P_w(s_i, \varphi_i, (x, y)))] dxdy,
\end{aligned} \tag{27}$$

$$\begin{aligned}
&\frac{1}{M\pi r_o^2} \sum_{j=1}^{M} \sum_{O_j^k \subseteq O_j} \mathbb{E}[\mathcal{U}(\sum_{\tilde{\varphi}_i \in \Gamma_3} \widetilde{P_w}(s_i, \tilde{\varphi}_i, O_j^k))] A(O_j^k) \\
&\geq \frac{1}{2} \cdot \frac{1}{M\pi r_o^2} \sum_{j=1}^{M} \sum_{O_j^k \subseteq O_j} \mathbb{E}[\mathcal{U}(\sum_{\tilde{\varphi}_i \in \Gamma_3^*} \widetilde{P_w}(s_i, \tilde{\varphi}_i, O_j^k))] A(O_j^k),
\end{aligned} \tag{28}$$

and

$$\begin{aligned}
&\frac{1}{M\pi r_o^2} \sum_{j=1}^{M} \sum_{O_j^k \subseteq O_j} \mathbb{E}[\mathcal{U}(\sum_{\varphi_i \in \Gamma_2^*} \widetilde{P_w}(s_i, \varphi_i, O_j^k))] A(O_j^k) \\
&- \frac{1}{M\pi r_o^2} \sum_{j=1}^{M} \sum_{O_j^k \subseteq O_j} \mathbb{E}[\mathcal{U}(\sum_{\tilde{\varphi}_i \in \Gamma_3^*} \widetilde{P_w}(s_i, \tilde{\varphi}_i, O_j^k))] A(O_j^k) \\
&\leq \frac{1}{M\pi r_o^2} \sum_{j=1}^{M} \sum_{O_j^k \subseteq O_j} \mathbb{E}[\mathcal{U}(\sum_{\varphi_i \in \Gamma_2^*} \widetilde{P_w}(s_i, \varphi_i, O_j^k))] A(O_j^k) \\
&- \frac{1}{M\pi r_o^2} \sum_{j=1}^{M} \sum_{O_j^k \subseteq O_j} \mathbb{E}[\mathcal{U}(\sum_{\tilde{\varphi}_i \in \Gamma_3^{*\prime}} \widetilde{P_w}(s_i, \tilde{\varphi}_i, O_j^k))] A(O_j^k)
\end{aligned}$$

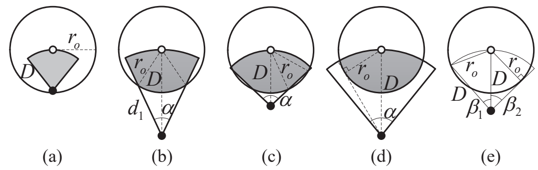

Fig. 6. Different cases of A_w and critical conditions: (a) $D \le r_o$, (b) $D > r_o$ and $\sin\frac{\alpha}{2} < \frac{r_o}{D}\sqrt{1-\frac{r_o^2}{2D^2}}$, (c) $D > r_o$ and $\frac{r_o}{D}\sqrt{1-\frac{r_o^2}{2D^2}} \le \sin\frac{\alpha}{2} < \frac{r_o}{D}$, (d) $D > r_o$ and $\sin\frac{\alpha}{2} \ge \frac{r_o}{D}$, (e) critical conditions

$$\begin{aligned}&\le \frac{1}{M\pi r_o^2}\sum_{j=1}^{M}\sum_{O_j^k,O_j^{k\prime}\subseteq O_j}(A(O_j^k)-A(O_j^{k\prime}))\\ &\le \frac{2N(D+r_o)}{\pi r_o}\Delta\varphi.\end{aligned} \tag{29}$$

First, if the orientations in Γ_3^* are far from those in Γ_2^*, there is certainly a solution $\Gamma_3^{*\prime}$ which is no better than Γ_3^* and the orientations in which are nearest to those in Γ_2^*. Since $\mathcal{U}(.)$ finally reaches 1, $\mathbb{E}[\mathcal{U}(\sum_{\varphi_i\in\Gamma_2^*}\widetilde{P_w}(s_i,\varphi_i,O_j^k))] \le 1$. According to Lemma IV.2, we know that the maximum sum of changing area of all the subareas covered by one charger is $2r_o(D+r_o)\Delta\varphi$ in one DDA. Thus, the maximum changing area in total for all N chargers is $2Nr_o(D+r_o)\Delta\varphi$, *i.e.*,

$$\sum_{O_j^k,O_j^{k\prime}\subseteq O_j}(A(O_j^k)-A(O_j^{k\prime})) \le 2Nr_o(D+r_o)\Delta\varphi \tag{30}$$

in every DDA. So, the result in Equation (29) stands.

We consider a real scenario that there are enough chargers to give the common charging area full charging utility, and the charger should be placed at the position where at least one center of a DDA is within distance D. The worst case is that all the chargers are placed at one point and with the same orientation, thus, makes the covering area harvest full charging utility. In this case, the average charging utility is $\frac{A_w}{M\pi r_o^2}$, where A_w is the covering area as shown in Figure 6(a)-(d) of Cases 1-4, and it is calculated by Equation (26). The critical conditions to differentiate Case 2, Case 3, and Case 4 are shown in Figure 6(e). In Case 3, there are two intersections on each line bound of the charging sector and the minimum $\frac{\alpha}{2}$ is β_1 as shown in 6(e), where $\cos\beta_1 = \frac{D^2+D^2-r_o^2}{2\times D\times D} = 1-\frac{r_o^2}{2D^2}$, so $\sin\beta_1 = \sqrt{1-\cos^2\beta_1} = \frac{r_o}{D}\sqrt{1-\frac{r_o^2}{2D^2}}$. The maximum $\frac{\alpha}{2}$ is obviously β_2 as shown in Figure 6(e) where $\sin\beta_2 = \frac{r_o}{D}$, that two line bounds of the charging sector are tangent to the DDA. Thus, in Case 3, $\sin\beta_1 \le \sin\frac{\alpha}{2} < \sin\beta_2$, that is, $\frac{r_o}{D}\sqrt{1-\frac{r_o^2}{2D^2}} \le \sin\frac{\alpha}{2} < \frac{r_o}{D}$. It is obvious that

$$\frac{1}{M\pi r_o^2}\sum_{j=1}^{M}\iint_{(x,y)\in O_j}\mathbb{E}[\mathcal{U}(\sum_{\varphi_i\in\Gamma_1^*}P_w(s_i,\varphi_i,(x,y)))]dxdy \ge \frac{A_w}{M\pi r_o^2}. \tag{31}$$

Thus,

$$\begin{aligned}&\frac{1}{M\pi r_o^2}\sum_{j=1}^{M}\sum_{O_j^k\subseteq O_j}\mathbb{E}[\mathcal{U}(\sum_{\varphi_i\in\Gamma_2^*}\widetilde{P_w}(s_i,\varphi_i,O_j^k))]A(O_j^k)\\ &-\frac{1}{M\pi r_o^2}\sum_{j=1}^{M}\sum_{O_j^k\subseteq O_j}\mathbb{E}[\mathcal{U}(\sum_{\tilde{\varphi}_i\in\Gamma_3^*}\widetilde{P_w}(s_i,\tilde{\varphi}_i,O_j^k))]A(O_j^k)\\ &\le \frac{2N(D+r_o)}{(A_w/(M\pi r_o^2))\pi r_o}\Delta\varphi\\ &\quad\cdot\frac{1}{M\pi r_o^2}\sum_{j=1}^{M}\iint_{(x,y)\in O_j}\mathbb{E}[\mathcal{U}(\sum_{\varphi_i\in\Gamma_1^*}P_w(s_i,\varphi_i,(x,y)))]dxdy\\ &= \frac{2MNr_o(D+r_o)}{A_w}\Delta\varphi\\ &\quad\cdot\frac{1}{M\pi r_o^2}\sum_{j=1}^{M}\iint_{(x,y)\in O_j}\mathbb{E}[\mathcal{U}(\sum_{\varphi_i\in\Gamma_1^*}P_w(s_i,\varphi_i,(x,y)))]dxdy.\end{aligned} \tag{32}$$

From Equation (27), (28) and (32), we have

$$\begin{aligned}&\frac{1}{1+\epsilon_1}\cdot\frac{1}{M\pi r_o^2}\sum_{j=1}^{M}\iint_{(x,y)\in O_j}\mathbb{E}[\mathcal{U}(\sum_{\varphi_i\in\Gamma_1^*}P_w(s_i,\varphi_i,(x,y)))]dxdy\\ &-2\cdot\frac{1}{M\pi r_o^2}\sum_{j=1}^{M}\sum_{O_j^k\subseteq O_j}\mathbb{E}[\mathcal{U}(\sum_{\tilde{\varphi}_i\in\Gamma_3}\widetilde{P_w}(s_i,\tilde{\varphi}_i,O_j^k))]A(O_j^k)\\ \le&\frac{1}{M\pi r_o^2}\sum_{j=1}^{M}\sum_{O_j^k\subseteq O_j}\mathbb{E}[\mathcal{U}(\sum_{\varphi_i\in\Gamma_2^*}\widetilde{P_w}(s_i,\varphi_i,O_j^k))]A(O_j^k)\\ &-\frac{1}{M\pi r_o^2}\sum_{j=1}^{M}\sum_{O_j^k\subseteq O_j}\mathbb{E}[\mathcal{U}(\sum_{\tilde{\varphi}_i\in\Gamma_3^*}\widetilde{P_w}(s_i,\tilde{\varphi}_i,O_j^k))]A(O_j^k)\\ \le&\frac{2MNr_o(D+r_o)}{A_w}\Delta\varphi\\ &\cdot\frac{1}{M\pi r_o^2}\sum_{j=1}^{M}\iint_{(x,y)\in O_j}\mathbb{E}[\mathcal{U}(\sum_{\varphi_i\in\Gamma_1^*}P_w(s_i,\varphi_i,(x,y)))]dxdy.\end{aligned} \tag{33}$$

Thus, we can bound the gap between the solutions to problem **P4** and **P1** as

$$\begin{aligned}&\frac{1}{M\pi r_o^2}\sum_{j=1}^{M}\sum_{O_j^k\subseteq O_j}\mathbb{E}[\mathcal{U}(\sum_{\tilde{\varphi}_i\in\Gamma_3}\widetilde{P_w}(s_i,\tilde{\varphi}_i,O_j^k))]A(O_j^k)\\ &\ge\frac{1}{2}\left(\frac{1}{1+\epsilon_1}-\frac{2MNr_o(D+r_o)}{A_w}\Delta\varphi\right)\\ &\quad\cdot\frac{1}{M\pi r_o^2}\sum_{j=1}^{M}\iint_{(x,y)\in O_j}\mathbb{E}[\mathcal{U}(\sum_{\varphi_i\in\Gamma_1^*}P_w(s_i,\varphi_i,(x,y)))]dxdy.\end{aligned} \tag{34}$$

Let $\epsilon_1 = \frac{\epsilon}{1-\epsilon}$ and $\Delta\varphi = \frac{A_w}{2MNr_o(D+r_o)}\epsilon$, then the approximation ratio of the algorithm is $\frac{1}{2}-\epsilon$.

We omit the time complexity analysis to save space. ■

V. Simulation Results

A. Evaluation Setup

In the simulations, we deploy both devices and chargers randomly in a $15\,\mathrm{m}\times 15\,\mathrm{m}$ square area such that the devices can only move in this area, *i.e.*, the moving centers of DDAs are randomly deployed in the center square with side length $(15-2r_o)\,\mathrm{m}$, and there must be at least one DDA center within

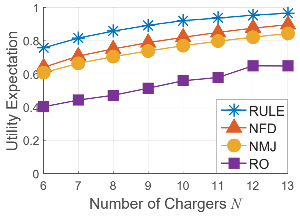

Fig. 7. N vs. $\mathbb{E}[\mathcal{U}]$

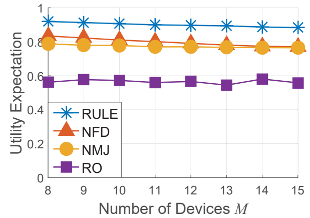

Fig. 8. M vs. $\mathbb{E}[\mathcal{U}]$

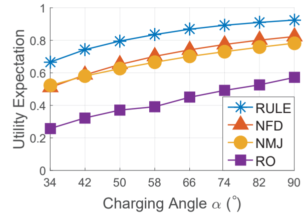

Fig. 9. α vs. $\mathbb{E}[\mathcal{U}]$

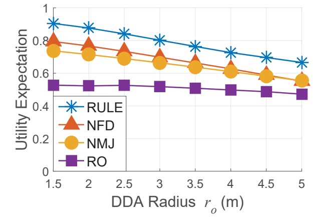

Fig. 10. r_o vs. $\mathbb{E}[\mathcal{U}]$

distance D with respect to a charger. The default settings of the parameters are: $D = 6\,\mathrm{m}$, $r_o = 2\,\mathrm{m}$, $M = 8$, $N = 10$, $a_1 = 100$, $b_1 = 5$, $a_2 = 4$, $b_2 = 3$, $\epsilon = 0.1$, and $P_{th} = 1.5W$.

As there is no existing algorithm can address our problem, we propose three algorithms for comparison. Randomized Orientations (RO) generates the orientations of the chargers randomly. No Moving or Jittering (NMJ) generates the orientations of the chargers by DCS extraction for point case algorithm as proposed in [3] with the assumption that $r_o = 0$, *i.e.*, the devices are fixed at their DDA centers, and there is no power jittering. Nearest Facing Device (NFD) selects the charger's nearest DDA center and makes the charger face it.

All results in the figures are the average utility expectations of 100 random deployments. We use Utility Expectation or $\mathbb{E}[\mathcal{U}]$ in the figures to denote the expectation of charging utility.

B. Performance Comparison

1) Impact of Number of Chargers N: Our simulation results show that on average RULE outperforms NFD, NMJ, and RO by 12.53%, 19.77%, and 68.91%, respectively, in terms of N. As shown in Figure 7, we test the expected charging utility with N from 6 to 13. All of these four algorithms achieve higher charging utility expectation with larger number of chargers. The increasing trend slows down when N becomes larger, since the expected charging utility is approximating the maximum expected charging utility of the specific topology gradually.

2) Impact of Number of Devices M: Our simulation results show that on average RULE outperforms NFD, NMJ, and RO by 12.85%, 16.42%, and 59.32%, respectively, in terms of M. We evaluate the expectation of charging utility when M varies from 8 to 15. The charging utility expectation of RULE, NFD, and NMJ decreases slowly with M becomes larger, while the results of RO fluctuate, as shown in Figure 8. Since the region is relatively small, the overall area of DDAs for chargers to cover will not become much larger as M increases and there will be more overlapped area of DDAs. The charging utility expectation of NFD decreases faster and finally reaches that of NMJ, while that of RO remains low.

3) Impact of Charging Angle α: Our simulation results show that on average RULE outperforms NFD, NMJ, and RO by 19.56%, 24.10%, and 103.25%, respectively, in terms of α. Charging angle α varies from $34°$ to $90°$ and the charging utility expectation of all the four algorithms increases fast when α increases as shown in Figure 9. Still, the increasing trend becomes slow when α becomes larger.

TABLE II
POSITIONS AND ORIENTATIONS OF CHARGERS

Index	Position	RULE	NFD	NMJ
1	$(51.31, 20.09)$	$51.6°$	$48.5°$	$78.5°$
2	$(140.29, 22.94)$	$80.2°$	$101.1°$	$76.1°$
3	$(182.53, 62.25)$	$40.1°$	$145.0°$	$121.7°$
4	$(50.13, 287.46)$	$326.6°$	$327.5°$	$357.5°$
5	$(148.82, 290.67)$	$51.6°$	$266.8°$	$296.8°$
6	$(273.39, 292.30)$	$80.2°$	$245.4°$	$76.1°$

4) Impact of DDA Radius r_o: Our simulation results show that on average RULE outperforms NFD, NMJ, and RO by 15.98%, 20.88%, and 54.36%, respectively, in terms of r_o. As shown in Figure 10, r_o increases from 1.5 to 5 and the charging utility expectation decreases when r_o increases and RULE, NFD, and NMJ decrease faster than RO.

VI. FIELD EXPERIMENTS

A. Testbed

As shown in Figure 11, our testbed consists of six TX91501 power transmitters produced by Powercast [26], [30]–[34], six rechargeable sensor nodes, and an AP connecting to a laptop to report the collected data. All the chargers and the devices are deployed in a $300\,\mathrm{cm} \times 300\,\mathrm{cm}$ square area, and the positions of the DDA centers are $(124.61, 102.84)$, $(235.97, 122.47)$, $(179.47, 167.46)$, $(239.54, 218.44)$, $(198.95, 221.39)$, and $(145.26, 226.89)$, and the positions of chargers are shown in Table II. The DDA radius r_o is $50\,\mathrm{cm}$ and $P_{th} = 30\,\mathrm{mW}$. To evaluate the charging utility expectation of a device in its DDA, we measured 17 points in each DDA, every $25\,\mathrm{cm}$ one point from the DDA center then add four points on the circle bound. We waited for at least $20\,\mathrm{s}$ at each point to collect enough data to calculate the expectation of charging utility.

B. Experimental Results

The scheduling strategies for RULE, NFD, and NMJ are shown in Table II and the visual ones are shown in Figure 12-14. From Figure 15, we can see that our algorithm RULE allows the charging utility expectation of each device roughly equal and relatively large, while that of the other two algorithms varies much for these devices. The CDF plot of all the data collection points is shown in Figure 16, and it shows that the line of RULE approaches 1 at the lowest speed, which indicates that the expectation charging utility of RULE is generally more than the other two.

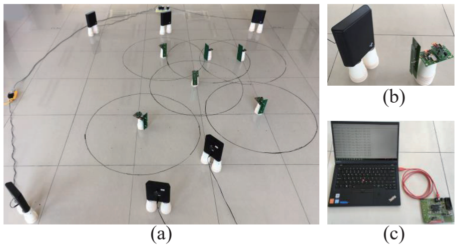

Fig. 11. Testbed: (a) Testbed; (b) Charger & device; (c) AP

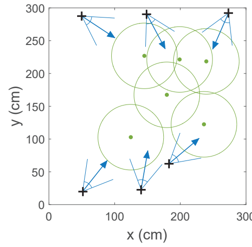

Fig. 12. RULE scheduling

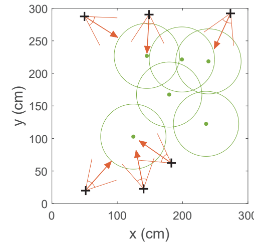

Fig. 13. NFD scheduling

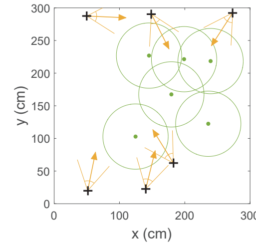

Fig. 14. NMJ scheduling

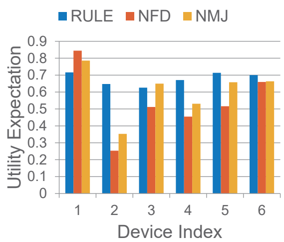

Fig. 15. $\mathbb{E}[\mathcal{U}]$ of different devices

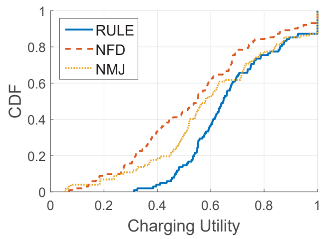

Fig. 16. $\mathbb{E}[\mathcal{U}]$ CDF of all points

VII. Conclusion

In this paper, we deal with the robust scheduling for wireless charger networks problem. The key novelty of this paper is on proposing the first scheme for robust wireless charger scheduling considering power jittering and device drifting. We establish the probabilistic model for charging power, apply area and orientation discretization, and conduct both simulation and field experiments. The key technical depth is to reformulate the objective function to a submodular function and bound the overall performance gap. Our experimental results show that our proposed method achieves good performance and can outperform comparison algorithms by 103.25% on average.

Acknowledgment

This work was supported in part by the National Key R&D Program of China under Grant No. 2018YFB1004704 and 2018YFB0803400, in part by the National Natural Science Foundation of China under Grant No. 61502229, 61872178, 61832005, 61672276, 61872173, 61321491, 61873177, 61772026, and 61332018, in part by the Natural Science Foundation of Jiangsu Province under Grant No. BK20181251, in part by the Fundamental Research Funds for the Central Universities under Grant 021014380079.

References

[1] "https://www.wirelesspowerconsortium.com/."

[2] H. Dai *et al.*, "Omnidirectional chargability with directional antennas," in *IEEE ICNP*, Nov 2016, pp. 1–10.

[3] ——, "Optimizing wireless charger placement for directional charging," in *IEEE INFOCOM*, May 2017, pp. 1–9.

[4] T. He *et al.*, "On using wireless power transfer to increase the max flow of rechargeable wireless sensor networks," in *IEEE ISSNIP*, April 2015, pp. 1–6.

[5] H. Dai *et al.*, "Radiation constrained scheduling of wireless charging tasks," *IEEE/ACM Transactions on Networking*, vol. 26, no. 1, pp. 314–327, Feb 2018.

[6] K. Xie *et al.*, "Low cost and high accuracy data gathering in wsns with matrix completion," *IEEE Transactions on Mobile Computing*, vol. 17, no. 7, pp. 1595–1608, 2018.

[7] ——, "An efficient privacy-preserving compressive data gathering scheme in wsns," *Information Sciences*, vol. 390, pp. 82–94, 2017.

[8] X. Lu *et al.*, "Wireless charging technologies: Fundamentals, standards, and network applications," *IEEE Communications Surveys Tutorials*, vol. 18, no. 2, pp. 1413–1452, Secondquarter 2016.

[9] R. Du *et al.*, "Flowing with the water: On optimal monitoring of water distribution networks by mobile sensors," in *IEEE INFOCOM*, April 2016, pp. 1–9.

[10] K. Xie *et al.*, "Quick and accurate false data detection in mobile crowd sensing," in *IEEE INFOCOM*, 2019.

[11] M. Erol-Kantarci *et al.*, "A survey of architectures and localization techniques for underwater acoustic sensor networks," *IEEE Communications Surveys Tutorials*, vol. 13, no. 3, pp. 487–502, Third 2011.

[12] J. A. Cobano *et al.*, "Data retrieving from heterogeneous wireless sensor network nodes using uavs," *Journal of Intelligent & Robotic Systems*, vol. 60, no. 1, pp. 133–151, Oct 2010.

[13] A. B. Noel *et al.*, "Structural health monitoring using wireless sensor networks: A comprehensive survey," *IEEE Communications Surveys Tutorials*, vol. 19, no. 3, pp. 1403–1423, thirdquarter 2017.

[14] H. Dai *et al.*, "Robustly safe charging for wireless power transfer," in *IEEE INFOCOM*, April 2018, pp. 1–9.

[15] S. Zhang *et al.*, "P^3: Joint optimization of charger placement and power allocation for wireless power transfer," in *IEEE INFOCOM*, April 2015, pp. 2344–2352.

[16] H. Dai *et al.*, "Safe charging for wireless power transfer," in *IEEE INFOCOM*, 2014, pp. 1105–1113.

[17] S. He *et al.*, "Energy provisioning in wireless rechargeable sensor networks," *IEEE Transactions on Mobile Computing*, vol. 12, no. 10, pp. 1931–1942, Oct 2013.

[18] L. Li *et al.*, "Radiation constrained fair wireless charging," in *IEEE SECON*, June 2017, pp. 1–9.

[19] H. Dai *et al.*, "Safe charging for wireless power transfer," *IEEE/ACM Transactions on Networking*, vol. 25, no. 6, pp. 3531–3544, Dec 2017.

[20] L. Li *et al.*, "Radiation constrained fair charging for wireless power transfer," *ACM Trans. Sen. Netw.*, Accepted.

[21] H. Dai *et al.*, "Radiation constrained scheduling of wireless charging tasks," in *ACM Mobihoc*, 2017, pp. 17:1–17:10.

[22] ——, "Wireless charger placement for directional charging," *IEEE/ACM Transactions on Networking*, vol. 26, no. 4, pp. 1865–1878, Aug 2018.

[23] N. Yu *et al.*, "Placement of connected wireless chargers," in *IEEE INFOCOM*, April 2018, pp. 387–395.

[24] X. Wang *et al.*, "Heterogeneous wireless charger placement with obstacles," in *ACM ICPP*, 2018, pp. 16:1–16:10.

[25] H. Dai *et al.*, "Charging task scheduling for directional wireless charger networks," in *ACM ICPP*, 2018, pp. 10:1–10:10.

[26] "http://www.powercastco.com/".

[27] L. He *et al.*, "icharge: User-interactive charging of mobile devices," in *ACM MobiSys*, 2017, pp. 413–426.

[28] Y. Zeng *et al.*, "Communications and signals design for wireless power transmission," *CoRR*, vol. abs/1611.06822, 2016.

[29] S. Fujishige, *Submodular functions and optimization*. Elsevier, 2005, vol. 58.

[30] H. Dai *et al.*, "Scape: Safe charging with adjustable power," in *IEEE ICDCS*, June 2014, pp. 439–448.

[31] ——, "Scape: Safe charging with adjustable power," *IEEE/ACM Transactions on Networking*, vol. 26, no. 1, pp. 520–533, Feb 2018.

[32] T. Wu *et al.*, "Collaborated tasks-driven mobile charging and scheduling: A near optimal result," in *IEEE INFOCOM*, 2019.

[33] H. Dai *et al.*, "Radiation constrained wireless charger placement," in *IEEE INFOCOM*, April 2016, pp. 1–9.

[34] T. Wu *et al.*, "Charging oriented sensor placement and flexible scheduling in rechargeable wsn," in *IEEE INFOCOM*, 2019.